ANNUAL REVIEWS

Annual Review of Condensed Matter Physics

Droplet Physics and Intracellular Phase Separation

Frank Jülicher[1,2] and Christoph A. Weber[3]

[1]Max Planck Institute for the Physics of Complex Systems, Dresden, Germany; email: julicher@pks.mpg.de

[2]Center for Systems Biology Dresden, Dresden, Germany

[3]Faculty of Mathematics, Natural Sciences, and Materials Engineering, Institute of Physics, University of Augsburg, Augsburg, Germany; email: christoph.weber@physik.uni-augsburg.de

Annu. Rev. Condens. Matter Phys. 2024. 15:237–61

First published as a Review in Advance on December 7, 2023

The *Annual Review of Condensed Matter Physics* is online at conmatphys.annualreviews.org

https://doi.org/10.1146/annurev-conmatphys-031720-032917

Keywords

biological condensates, emulsion, membraneless compartments, active droplets, phase coexistence

Abstract

Living cells are spatially organized by compartments that can nucleate, grow, and dissolve. Compartmentalization can emerge by phase separation, leading to the formation of droplets in the cell's nucleo- or cytoplasm, also called biomolecular condensates. Such droplets can organize the biochemistry of the cell by providing specific chemical environments in space and time. These compartments provide transient environments, suggesting the relevance of nonequilibrium physics of droplets as a key to unraveling the underlying physicochemical principles of biological functions in living cells. In this review, we highlight coarse-grained approaches that capture the physics of chemically active emulsions as a model for condensates orchestrating chemical processes. We also discuss the dynamics of single molecules in condensates and the material properties of biological condensates and their relevance for the cell. Finally, we propose wetting, prewetting, and surface phase transitions as a possibility for intracellular surfaces to control biological condensates, spatially organize membranes, and exert mechanical forces.

Centrosomes: dense assemblies of proteins that serve as organizing centers for the microtubule networks in cells

Centrioles: protein complexes located at the center of centrosomes that have a well-defined structure and are duplicated after cell division

Nucleolus: an organelle inside the cell nucleus where ribosomes are assembled

Ribosomes: molecular machines that are complexes of several proteins and RNA; they assemble proteins, reading the genetic code of messenger RNA

1. INTRODUCTION: BIOLOGICAL CONDENSATES AS A PHASE SEPARATION PHENOMENON

1.1. Membraneless Compartments in Cell Biology

Living cells exhibit a complex architecture (1). The cell's biochemistry is spatially organized, and the cell forms and maintains compartments that separate distinct biochemical environments (see **Figure 1** for an illustration). The classic example is membrane bound compartments. Membranes provide boundaries for many organelles and present barriers for many molecules that do not pass the membrane in the absence of specific molecular channels, pumps, and transporters. Interestingly, many biochemical compartments are not membrane bound (2, 3). Key examples are the centrosome, which is a dense material formed around centrioles (4, 5), and the nucleolus, in which components of ribosomes are assembled (6–8). An important breakthrough was the discovery that many membraneless compartments can behave as liquid droplets in the cell: They can deform, fuse, and relax to a spherical shape. This discovery was initially made for P granules (9) and later also for the nucleolus (6). P granules are assemblies of proteins and RNA that play a role in the specification of the germ line of the round worm *Caenorhabditis elegans* (10). In the fertilized egg of the worm, dozens of P granules of different sizes are homogeneously distributed in the cytoplasm.

During the process of the first cell division, P granules segregate to the posterior side and end up only in the posterior daughter cell, a precursor to the germ line (11). This P granule segregation can be understood as a position-dependent phase separation process (9, 12, 13). A concentration gradient of the protein MEX-5 in the cell forms via a spatially segregated kinase/phosphatase cycle (14) and induces the dissolution of P granules at the anterior side of the cell and the condensation of RNA-protein-rich droplets, the P granules, at the posterior side (15). The observation of droplets, particularly droplet dissolution and growth, suggests a phase separation phenomenon underlying the formation of membraneless compartments. To emphasize the soft matter aspects of membraneless compartments in cells, they are also referred to as biological condensates (16, 17).

Many intracellular condensates are assemblies of proteins and RNA (16, 18). This is the case for P granules and nucleoli, Cajal bodies, and PML bodies in the nucleus and stress granules and P bodies in the cytoplasm (16). Often they exhibit the properties that we know from liquids; i.e.,

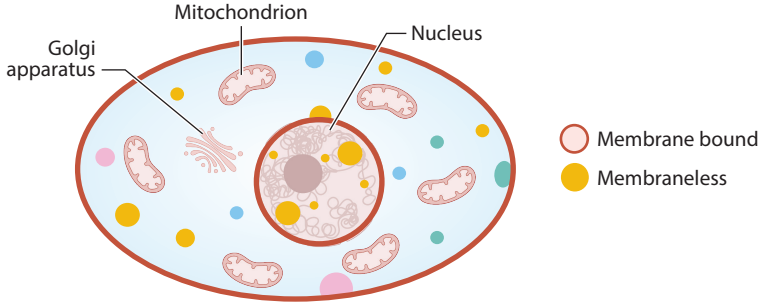

Figure 1

Illustration of membrane bound and membraneless organelles in a cell. Cells are spatially organized via membrane bound and membraneless compartments. Membrane bound compartments such as mitochondria, the Golgi apparatus, and the cell nucleus are surrounded by a membrane (*red boundary*). In contrast, membraneless organelles lack a membrane. They have condensed phases that coexist with their surroundings and are also called biomolecular condensates. They often share physical properties with phase-separated droplets. For example, they can fuse, exchanging molecules by diffusion through their interface, and they can interact with membrane surfaces, leading to wetting, or condensation on filaments and cocondensation.

they are very dynamic, and their components quickly exchange through the condensate interface. These properties were revealed by single-molecule studies (19) and fluorescence recovery after photobleaching of fluorescently labeled molecules (9, 20, 21). Furthermore, condensates are often spherical. They fuse upon contact and form a larger condensate that relaxes to a spherical shape (9, 22). These observations provide evidence for the effects of surface tension, which is a generic property of interfaces separating two coexisting liquid phases. The slowest timescale $\tau = \eta R/\gamma$ of the shape relaxation to a spherical shape of radius R is set by viscosity η and surface tension γ given R. Viscosity is related to the diffusion coefficient of molecules $D \simeq k_B T/(6\pi\eta a)$, where a is a molecular size.

The fact that many condensates are liquid and molecules can diffuse quickly implies that chemical reactions can occur in the condensate volume, where all reacting species meet. Therefore, small droplet compartments can serve as microreactors (23), localizing and regulating biochemical processes (24–26). Droplets are phases that coexist with an outside phase. Phases are separated by interfaces at which concentrations can change abruptly. Chemically reacting components can accumulate inside the droplets or during the outside phase, respectively. The different concentrations can facilitate or suppress chemical processes (27–29) and thereby enable certain biological functions in living cells (26, 30–32).

Phase separation is governed by the laws of thermodynamics, reflecting the competition between entropy and energy. Equilibrium between phases is governed by equal chemical potentials. At the phase boundaries, concentrations change abruptly, whereas chemical potentials vary smoothly. Gradients of chemical potential give rise to molecular diffusion from one phase to the other. The composition jumps across a phase boundary when moving from one phase to the other can be characterized by partition coefficients. They describe the concentration ratios of the individual components. A value unequal to one reflects that components are partitioned unequally between phases. Cells can use this partitioning of reacting molecules to organize biochemistry, for example, to position specific enzymes in a specific condensate (33) or to localize biochemical processes such as metabolic pathways (34).

Droplet formation occurs when the concentration of a component exceeds the saturation concentration above which coexisting phases can be nucleated (35–37). Strikingly, nucleation of biomolecular condensates in living cells can be described by classical nucleation theory despite the multicomponent and highly complex intracellular environment (38). The saturation concentration above which nucleated condensates grow depends in general on temperature, pH, salt, and composition (39–42). Therefore, a regulator component can influence condensate formation or dissolution in a concentration-dependent manner. If the regulator establishes a concentration gradient, droplets can be positioned, as they may grow in one region and dissolve in another (12, 13). Such droplet positioning was shown, for example, for P granule droplets segregating to the posterior part of the cell (9).

Chemical processes in cells are maintained away from thermodynamic equilibrium due to the continuous influx or efflux of energy and mass associated with a production of entropy (43, 44). As a consequence, condensates in cells that organize chemical processes represent a nonequilibrium system. Such chemically active droplets can exhibit unconventional behaviors, such as suppressed Ostwald ripening (45–47) and instabilities that can lead to spontaneous droplet division (48, 49) or the formation of liquid spherical shells (50). Also, such chemically active droplets produce entropy and can release heat (51), revealing the rich physical properties of such chemically active emulsions (37, 52).

The examples discussed suggest that multicomponent mixtures away from thermodynamic equilibrium give rise to a rich collective behavior of molecules. Such collective behaviors can be used by cells to generate mesoscopic structures that organize biochemistry in space as an

Kinase: a biological catalyst, i.e., enzyme, that catalyzes the attachment of a phosphate group to a protein

Phosphatase: a biological catalyst, i.e., enzyme, that catalyzes the detachment of a phosphate group

Chromatin: a polymeric material where DNA in the cell nucleus is packed together with proteins

Transcription factors: proteins that regulate the expression of a gene

alternative to the pairwise binding of molecules (53), or the formation of molecular complexes of specific structures, such as the nuclear pore complex or ribosomes.

Assemblies of molecules that emerge as a phase separation phenomenon could play a vital role in the cell nucleus in chromatin organization (54–56) and regulation of gene expression (31, 57–59). For example, during the transcription of a gene, a messenger RNA molecule is generated. RNA binding proteins and the produced RNA could phase-separate from the background chromatin. Transcription factors and other associated proteins could condense on DNA and form condensates that recruit proteins that regulate gene expression. Finally, there is evidence that the distinction between dense heterochromatin and more open euchromatin could emerge from phase separation that involves histones guided by epigenetic modifications (60).

These examples reveal that the physics of phase separation can play an essential role in a cell by providing a mechanism for complex spatial organization. However, the scenarios in a cell are much more complex than simple liquid-like droplets, as many components are involved, nonequilibrium conditions are the norm, and molecular components are complex macromolecules or long polymers that add an extra level of complexity. Therefore, many new phenomena are expected to be discovered in the study of the collective organization of membraneless compartments.

A key question is how condensates in cells can stay small, even though phase-separated droplets tend to coarsen and grow in size. Small sizes could be achieved by nonequilibrium conditions such as turnover (40, 46, 51, 61) or via the emergence of microphase separation as can be found in complex polymer and protein systems (62, 63). Fluctuations govern small-scale structures. It is an exciting question to understand down to what sizes the physical picture of droplets remains a valuable concept for small condensates. This question is particularly important for droplet formation inside organelles such as the nucleus.

An important element for the organization of small condensates in cells is the condensation on surfaces such as membranes (64–67) or polymers such as DNA (68–70). If molecules bind to a surface, they can act as precursors to phase separation at concentrations below the saturation concentration at which droplets can form in bulk (65). For example, thin adsorbed layers can form at low concentrations, and suddenly, a transition to a thick condensate can occur for increasing concentrations while remaining below bulk phase separation. Such prewetting phenomena are mesoscopic analogs of bulk phase separation controlled by surfaces. We expect cells to use the rich range of possible behaviors arising when many molecules interact. In the following sections, we discuss aspects of the physics of liquid phase separation relevant to cells.

1.2. Molecular Interactions and Phase Coexistence

Molecular interactions among molecules govern phase separation and the formation of condensed droplets. In thermodynamics, such interactions are described by a free energy. For a system in which temperature T, system volume V, and the number of molecules N are fixed, this is the Helmholtz free energy $F = Vf$, where f denotes the corresponding free energy density. For a simple binary mixture, the Helmholtz free energy density within the mean field approximation reads as (71–73)

$$f(T,\phi) = \frac{k_B T}{\nu_0(T)}\left[\frac{\phi}{\xi(T)}\log\phi + (1-\phi)\log(1-\phi) + \omega(T)\phi + \frac{\chi(T)}{k_B T}\phi(1-\phi)\right], \qquad 1.$$

where $\phi = \nu N/V$ denotes the volume fraction of solute molecules in a solvent with volume fraction $(1-\phi)$. Furthermore, the molecular volume of solvent and solute is denoted by $\nu_0(T)$ and $\nu(T) = \xi(T)\nu_0(T)$, which in general can be temperature dependent. Internal degrees of freedom are captured by the relative internal free energy $\omega(T)$ between the solute molecule and solvent. Interactions between both types of molecules are described by the interaction parameter $\chi(T)$.

The relative internal free energy $\omega(T)$ and the interaction parameter $\chi(T)$ can be decomposed into an enthalpic, temperature-independent, and an entropic contribution that scales with temperature (40, 74, 75). The free energy (Equation 1) can be obtained by a mean-field approximation (37, 76), leading to interaction terms up to the second order in ϕ. The random phase approximations allow us to go beyond the mean field (74, 76) and even account for sequence properties (77, 78).

Once the solute molecules described by the volume fraction ϕ are nondilute, i.e., the system is crowded, the system may phase-separate, leading to coexisting phases at thermodynamic equilibrium. To understand which molecular interactions, characterized by the parameter $\chi(T)$, can cause phase separation, we calculate the binodal for the binary mixture. The binodal corresponds to the concentration beyond which phases can coexist; it is often referred to as saturation concentration. In a binary incompressible mixture, two phases can coexist. This follows from a general argument: An M-component, incompressible mixture with P phases has $(M-1)P$ unknown phase concentrations. There are $M(P-1)$ phase equilibrium conditions, giving $(M-P)$ remaining degrees of freedom; this counting is often referred to the Gibbs phase rule. The maximal number of coexisting phases occurs for zero degrees of freedom. Thus, an incompressible M-component mixture can have maximally M coexisting phases. Indicating the two coexisting phases as I and II, with $\phi^{\mathrm{I}} > \phi^{\mathrm{II}}$, the binodal concentration is governed by the conditions for phase equilibrium: equal temperatures $T^{\mathrm{I}} = T^{\mathrm{II}}$, equal osmotic pressures $\Pi^{\mathrm{I}} = \Pi^{\mathrm{II}}$, and equal exchange chemical potentials $\bar{\mu}_i^{\mathrm{I}} = \bar{\mu}_i^{\mathrm{II}}$. Here, the osmotic pressure $\Pi = f - \phi\bar{\mu}/\nu$ and the exchange chemical potential $\bar{\mu} = \nu\partial f/\partial\phi$ are related to the free energy density f and, thus, to the molecular interactions and the molecular volume of solute ν and solvent ν_0.

For the simple free energy density given by Equation 1, the equilibrium concentrations ϕ^{I} and ϕ^{II} are given for the case of equal molecular volumes of solute and solvent ($\xi = 1$) by $\chi(\phi) = k_{\mathrm{B}}T\ln(\phi/(1-\phi))/(2\phi-1)$ with a critical point at $\phi^{\mathrm{I}} = \phi^{\mathrm{II}} = \phi_{\mathrm{c}} = 1/2$. The relation $\chi(\phi)$ for the equilibrium concentrations suggests that the saturation concentration ϕ^{II} decreases as the interaction parameter χ increases following an exponential, $\phi^{\mathrm{II}} \sim \exp(-\chi/(k_{\mathrm{B}}T))$ for large χ. In other words, enhancing the interaction parameter by $2k_{\mathrm{B}}T$ leads to a roughly tenfold decrease in the saturation concentration. This strong dependence is consistent with the large range of saturation concentrations from micromoles to millimoles observed for in vitro (79) and in vivo (73, 80) phase separating systems with interactions ranging from weak (few $k_{\mathrm{B}}T$) to stronger interactions such as hydrogen bonds (about $10k_{\mathrm{B}}T$). For proteins in an aqueous environment, solute molecular volumes are much larger than the solvent ($\xi \gg 1$). For increasing ξ, the binodal gets skewed toward smaller volume fractions. A necessary condition for phase separation is that interaction parameter χ is above the critical interaction parameter $\chi_{\mathrm{c}} = (k_{\mathrm{B}}T/2)(\xi^{-1/2}+1)^2$ (41). It depends on ξ, implying that for the case of large macromolecules in water, $\chi_{\mathrm{c}} \simeq k_{\mathrm{B}}T/2$. At the critical point, the volume fractions of coexisting phases become equal $\phi^{\mathrm{I}} = \phi^{\mathrm{II}} = \phi_{\mathrm{c}}$ with $\phi_{\mathrm{c}} = 1/(1+\xi^{1/2})$, which moves to smaller values for increasing ξ.

The chemical potential describes the slope of the free energy density as a function of ϕ. Therefore, the conditions of equal chemical potentials and equal osmotic pressures for the solutions of the phase equilibrium correspond graphically to a Maxwell construction. In this construction, the partially nonconvex free energy gets replaced by a convex hull to the free energy density f, where the zero-curvature contours of the hull are the domains in which two phases can coexist.

Whereas a thermodynamic phase diagram is strictly only valid for (infinitely) large systems, the Maxwell construction is altered for finite systems. The reason is that finite phases can now have curved interfaces, and the energetic contributions of the interface to the free energy proportional to surface tension can be significant. For spherical droplets of radius R, the combined effects of curvature $1/R$ and surface tension γ are governed by the Laplace pressure, $p = 2\gamma/R$. The surface

tension can be approximately expressed in terms of molecular parameters (37), $\gamma \simeq k_B T \chi^{1/2}(\chi - 2)^{3/2}/(2\nu^{2/3})$. This surface contribution to the free energy increases the equilibrium concentration in both phases, which is described by the Gibbs–Thomson relationship $\phi^{I/II}(R) = \phi_0^{I/II}(1 + \ell/R)$. Here, $\phi_0^{I/II}$ denotes the equilibrium volume fraction for infinitely large phases, and ℓ denotes the capillary length. The concentration increase relative to infinite systems scales with ℓ/R. For large χ, the capillary length scales as $\ell \sim \chi^{1/2}(\chi - 2)^{3/2}\nu^{1/3}$ (37). This relationship suggests that the capillary length is of the order of a molecule diameter, $\nu^{1/3}$, and is thus typically smaller than the mesoscopic droplet size. Even though the effect of curvature on the equilibrium concentrations is very small, these differences give rise to the relaxation of a deformed droplet to its spherical shape. Furthermore, such differences drive coarsening of the droplet size distribution referred to as Ostwald ripening during which bigger drops grow at the expense of smaller shrinking drops that eventually disappear. Thus, in cells, curvature effects are relevant because many membraneless organelles are almost spherical (2, 3), and there is evidence for coarsening processes in cells (81).

1.3. Phase Separation in the Cell Governed by Nonequilibrium Thermodynamics

In the previous section, we provided the thermodynamic definition of phases at equilibrium. We also introduced coexisting phases and droplets as a mechanism to organize different molecular components in living cells. Here, we ask whether intracellular droplets are phases in equilibrium with the cytoplasmic environment. Strictly speaking, the answer is no, because metabolic processes maintain chemical reactions and, thus, also phase separation in cells is out of equilibrium. For example, cells hydrolyze on average approximately a million ATP or GTP molecules per second in a volume of 1 $(\mu m)^3$ to maintain chemical processes out of equilibrium (82). Examples are the phosphorylation of proteins and the transport of cellular cargo dragged by molecular machines along filaments. Each hydrolysis event releases about $10 k_B T$ of heat. Though the resulting temperature gradient toward the cell's membrane is negligible, a large number of exothermal chemical events lead to local fluctuations in temperature that can cause deviation to thermodynamic equilibrium on a short timescale and length scale (83). A single hydrolysis event can cause a temperature upshift of a few Kelvin on the nanometer scale; however, this temperature increase fades away on tens and hundreds of nanometers due to the fast heat transport in aqueous media like the cell. On these length scales, the effects of nonequilibrium metabolic reactions are negligible; thus, local thermodynamic equilibria establish (see **Figure 2** for an illustration). On even larger scales, presumably micrometers and above, nonequilibrium effects can emerge that are characterized by diffusive and chemical fluxes and spatial gradients in concentrations. The fact that local thermodynamic equilibria can hold was shown for P granules in the *C. elegans* embryo (73). In these studies, the compositions inside and outside of P granule droplets were measured for different ambient temperatures. The result was the first phase diagram for biomolecular condensates in a living cell.

The applicability of local phase separation equilibria in living cells would have several implications. First, accurately measuring local concentrations inside and outside of intracellular condensates yields, except for the presumably weak effects of Laplace pressure, the equilibrium concentrations and the phase diagram. This diagram quantifies how strong molecules interact in living cells. Second, the relevance of thermodynamics for phase separation in living cells suggests applying thermodynamic perturbations to characterize how cells control droplet formation through concentration gradients and membrane surfaces. An interesting application is laser-induced temperature gradients that perturb protein concentration gradients in dividing

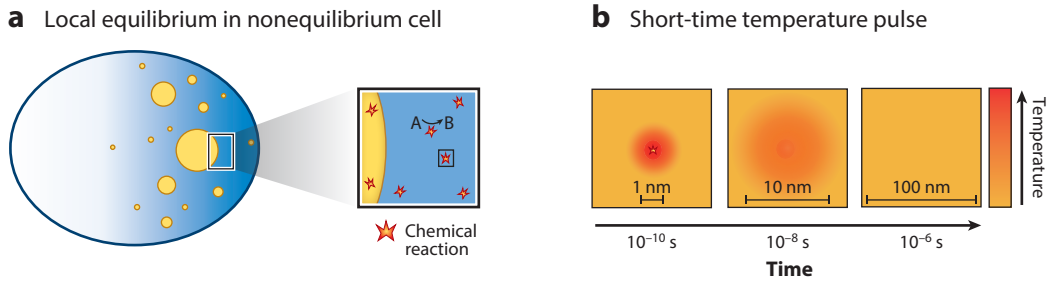

Figure 2

Local equilibria in living cells. (*a*) The cell is out of equilibrium. Signatures of its nonequilibrium nature are, for example, concentration gradients and the coexistence of many droplets. Nonequilibrium conditions emerge, for example, due to chemical reactions driven by the hydrolysis of ATP or GTP. (*b*) Each hydrolysis event gives rise to a heat pulse (*red star*), leading to a temperature pulse. The resulting temperature profile with an initial temperature increase on the order of Kelvins after a picosecond on the scale of a molecule (nanometer) spreads and decays quickly. Thus, on length scales around 100 nanometers, local equilibrium is established on timescales above about a microsecond.

cells (84). Finally, the intracellular phase separation dynamics can be well described by theoretical approaches relying on local equilibrium, such as Onsager's irreversible thermodynamic theory (85). Here, we review how coarse-grained approaches relying on irreversible thermodynamics can be used to decipher new physical phenomena in phase-separated systems that are maintained away from thermodynamic equilibrium by chemical reactions.

2. CHEMICALLY ACTIVE EMULSIONS

Emulsions are phase-separated liquid mixtures that are spatially inhomogeneous with droplets immersed in a background phase. Often such emulsions are dynamic, and the size distributions of droplets and their numbers change with time. A key example is Ostwald ripening, which leads to a steady increase in average droplet size while small droplets shrink and dissolve. Emulsions can be either passive when a phase separating system coarsens to reach equilibrium (86, 87) or active when energy is injected at small scales that maintain the system out of equilibrium and microscopic reversibility is broken (88–91).

Here, we review the nonequilibrium thermodynamic principles (43, 92) governing emulsions in which phase separation occurs in the presence of chemical reactions and local equilibrium holds. Such systems are passive when reactions tend toward chemical equilibrium, but can be active, if chemical equilibrium is prevented by boundary conditions or coupling to reservoirs and chemostats.

2.1. Thermodynamics of Liquid Mixtures with Chemical Reactions

We consider a system of $(M+1)$ components with concentrations $n_i = N_i/V$, where $i = 0, \ldots, M$, and N_i denote the molecule numbers of species i in the volume V. We develop our theory based on local thermodynamic equilibrium using the Gibbs free energy $G(N_i, T, p)$ as thermodynamic potential, where the particle number N_i, the temperature T, and the pressure p are fixed. The volume $V = \partial G/\partial p$ can be expressed as $V = \sum_{i=0}^{M} \nu_i N_i$, where $\nu_i = \partial V/\partial N_i = \partial \mu_i/\partial p$ are molecular volumes that are constant and independent of pressure in incompressible systems. The chemical potentials are defined as $\mu_i = \partial G/\partial N_i$. The entropy is $S = -\partial G/\partial T$. For a homogeneous system, the G is extensive, implying $G = \sum_{i=0}^{M} \mu_i N_i$ and $S = \sum_{i=0}^{M} s_i N_i$, with $s_i = -\partial \mu_i/\partial T$ being the entropy per molecule. The Helmholtz free energy reads as $F = G - pV = E - TS$, where E is the internal energy. We also define the enthalpy, $H = E + pV = G + TS$.

In incompressible systems, chemical potentials can be written as

$$\mu_i = k_B T \ln(n_i \gamma_i) + \mu_i^0 + \nu_i p, \qquad 2.$$

where μ_i^0 are reference chemical potentials, and the functions $\gamma_i(n_k, T)$ are often called activity coefficients. The exchange chemical potentials are defined relative to the solvent, $\bar{\mu}_k = \mu_k - \mu_0 \nu_k / \nu_0$, $k = 1, \ldots, M$.

Each component occupies a fraction $\phi_i = n_i \nu_i$ of the volume V with $\sum_{i=0}^{M} \phi_i = 1$. Without loss of generality, we specify ϕ_0 to denote the solvent volume fraction. We write chemical reactions $\alpha = 1 \ldots R$ in the form

$$\sum_{i=0}^{M} \sigma_{i\alpha}^{+} C_i \rightleftharpoons \sum_{i=0}^{M} \sigma_{i\alpha}^{-} C_i, \qquad 3.$$

where C_i is the chemical symbol of species i, and $\sigma_{i\alpha}^{\pm}$ are stoichiometric matrices, and we also define $\sigma_{i\alpha} = \sigma_{i\alpha}^{+} - \sigma_{i\alpha}^{-}$. The Gibbs free energy change per single event of reaction α is $\Delta G_\alpha = G_\alpha^{-} - G_\alpha^{+}$, which is the difference in the Gibbs free energy of products G_α^{-} and of the educts G_α^{+}, where

$$G_\alpha^{\pm} = \sum_{i=0}^{M} \sigma_{i\alpha}^{\pm} \mu_i. \qquad 4.$$

2.2. Phase Equilibrium and Chemical Equilibrium

Two phases I and II with different composition n_i^{I} and n_i^{II} coexist at phase equilibrium when all chemical potentials and temperatures are equal, $\mu_i^{\mathrm{I}} = \mu_i^{\mathrm{II}}$ and $T^{\mathrm{I}} = T^{\mathrm{II}}, p^{\mathrm{I}} = p^{\mathrm{II}}$. Although chemical potentials vary gently at phase boundaries, the concentrations change abruptly when moving between phases. The partitioning of molecules of species i in two coexisting phases is described by the partition coefficient $P_i = n_i^{\mathrm{I}} / n_i^{\mathrm{II}}$, which specifies the concentration ratio in the two phases separated by an interface that is at local equilibrium. The partition coefficient can be expressed in terms of the activity coefficients in the two phases $P_i = \gamma_i^{\mathrm{II}} / \gamma_i^{\mathrm{I}}$. When a spherical droplet of phase II with radius R coexists in an environment of phase I, mechanical equilibrium requires a Laplace pressure difference $p^{\mathrm{II}} = p^{\mathrm{I}} + 2\gamma/R$, where γ denotes surface tension. The exchange of molecules between phases is equilibrated when all exchange chemical potentials are equal, $\bar{\mu}_k^{\mathrm{I}} = \bar{\mu}_k^{\mathrm{II}}$, even if the pressures p^{I} and p^{II} differ. In this case, partitioning of molecules between droplet and environment is described by the partition coefficient

$$P_i = \frac{\gamma_i^{\mathrm{II}}}{\gamma_i^{\mathrm{I}}} \exp\left(\frac{\nu_i (p^{\mathrm{II}} - p^{\mathrm{I}})}{k_B T} \right). \qquad 5.$$

Chemical equilibrium is reached when the reaction Gibbs free energies vanish, $\Delta G_\alpha = 0$. This condition can be written by introducing an equilibrium coefficient of reaction α defined as $K_\alpha = \prod_{i=0}^{M} (n_i)^{\sigma_{i\alpha}}$, where n_i are the equilibrium concentrations of the reactions. In dilute solutions, K_α become equilibrium constants of reactions. Because both phase and thermodynamic equilibria are governed by the same chemical potentials, there is a relationship between reaction coefficients in the two phases and the partition coefficients (28, 93):

$$\frac{K_\alpha^{\mathrm{I}}}{K_\alpha^{\mathrm{II}}} = \prod_{i=0}^{M} (P_i)^{\sigma_{i\alpha}}. \qquad 6.$$

This relation shows that chemical reaction equilibria differ inside and outside a droplet phase, and this needs to be taken into account when using mass action kinetics in phase separating systems (28).

2.3. Dynamic Equations for Chemically Active Emulsions

In this section, we consider spatially inhomogeneous and incompressible systems and introduce the Gibbs free energy density,

$$G = \int_V d^3x\, g(n_i, \nabla n_i, T, p) \quad \text{with} \quad g(n_i, \nabla n_i, T, p) = f(n_i, \nabla n_i, T) + p. \tag{7.}$$

Here, $f = f_0(n_i, T) + (1/2)\sum_{ij}\kappa_{ij}\nabla n_i \cdot \nabla n_j$ denotes the Helmholtz free energy density with $f_0(n_i, T)$ being the homogeneous free energy density. The matrix κ_{ij} characterizes the costs due to concentration gradients. The chemical potentials are now defined as $\mu_i = \delta G/\delta n_i$. We define the entropy density $s = -\partial f/\partial T$ and determine the energy density as $e = f + sT$. The enthalpy density is then given as $h = g + Ts = e + p$. Furthermore, we introduce the entropy per molecule $s_i = -\partial \mu_i/\partial T$ and the enthalpy per molecule $h_i = \mu_i + Ts_i$. Finally, we also define exchange chemical potentials $\bar{\mu}_i = \mu_i - \nu_i\mu_0/\nu_0$ describing the Gibbs free energy change when molecules are exchanged with solvent of the same volume.

We write the balance equation of concentrations as

$$\partial_t n_i + \nabla \cdot \mathbf{j}_i = r_i, \tag{8.}$$

where $\mathbf{j}_i$ are the diffusion fluxes of molecules with $\sum_{i=0}^{M} \nu_i \mathbf{j}_i = 0$, and

$$r_i = -\sum_{\alpha=1}^{R} \sigma_{i\alpha} r_\alpha \tag{9.}$$

is the source rate per volume of molecules of species i from chemical reactions, where r_α denotes the net rate per volume of reaction α. Dynamic equations can be obtained using irreversible thermodynamics built from the expression of the rate of entropy production per volume $\dot{\theta}$ with

$$T\dot{\theta} = -\sum_{i=1}^{M} \mathbf{j}_i \cdot \nabla \bar{\mu}_i - \sum_{\alpha=1}^{R} r_\alpha \Delta G_\alpha - \mathbf{j}_s \cdot \nabla T, \tag{10.}$$

where $\mathbf{j}_s$ is the entropy flux. The three terms on the right represent products of pairs of conjugate thermodynamic forces and fluxes. To linear order in the forces, fluxes and forces are related by Onsager relations:

$$\mathbf{j}_i = -\sum_{j=1}^{M} \Lambda_{ij} \nabla \bar{\mu}_j - \Gamma_i \nabla T, \tag{11.}$$

$$\mathbf{j}_s = -\sum_{i=1}^{M} \Gamma_i \nabla \bar{\mu}_i - \Lambda \nabla T, \tag{12.}$$

where the coefficients $\Lambda_{ij} = \Lambda_{ji}$ describe diffusion, Γ_i accounts for the coupling between heat flow and particle flux, and Λ is related to heat conduction. The matrix of diffusion coefficients can be obtained as $\hat{D}_{ij} = \sum_{i=k}^{M} \Lambda_{ik}\partial \bar{\mu}_k/\partial n_j$, whereas thermophoresis is described by the coefficient $\zeta_i = \sum_j \Lambda_{ij}\partial \bar{\mu}_j/\partial T + \Gamma_i$. Chemical reaction rates can be written as

$$r_\alpha = k_\alpha \left(\exp\left[\frac{G_\alpha^+}{k_B T}\right] - \exp\left[\frac{G_\alpha^-}{k_B T}\right] \right), \tag{13.}$$

where the kinetic rate per volume k_α can depend on composition, temperature, and pressure. Note that Equation 13 obeys linear Onsager relations for small $\Delta G_\alpha = G_\alpha^- - G_\alpha^+$. It can be motivated in the nonlinear regime from the detailed balance condition,

$$\frac{r_\alpha^+}{r_\alpha^-} = \exp\left(-\frac{\Delta G_\alpha}{k_B T}\right), \tag{14.}$$

relating forward and backward reaction rates $r_\alpha^\pm$ with $r_\alpha = r_\alpha^+ - r_\alpha^-$ and from which Equation 13 follows. For passive systems, the dynamic equations lead to relaxation to thermodynamic equilibrium. The system can be maintained away from equilibrium by coupling to reservoirs. One scenario entails fixed concentration boundary conditions, where molecules exchange with reservoirs and reservoir concentrations remain fixed. Another scenario is coupling to chemostats, where chemical potentials of some species are imposed that can drive chemical reactions. Both situations lead to the physics of active emulsions in which unconventional behaviors emerge, such as suppressed Ostwald ripening (46, 47), or droplet instabilities, such as spontaneous division (48, 49, 51).

2.4. Entropy and Energy Balance

When studying active emulsions, conservation laws and the first and second laws of thermodynamics provide an important conceptual framework to address how energy and matter flow through the system (51). The first law of thermodynamics describes the conservation of energy and the exchange of heat and work of a system with its environment. The conservation law can be written in terms of the energy density e, as

$$\partial_t e + \nabla \cdot \mathbf{j}_\mathrm{e} = 0, \tag{15.}$$

where the energy flux $\mathbf{j}_\mathrm{e} = \mathbf{j}_\mathrm{h} + \mathbf{j}_\mathrm{q}$ is the sum of an enthalpy flux $\mathbf{j}_\mathrm{h}$ and the heat flux $\mathbf{j}_\mathrm{q}$. The energy density $e = f + Ts = g + Ts - p$ can also be expressed via the enthalpy per molecule as $e = \sum_{i=0}^{M} n_i h_i - p$. The enthalpy flux is given by $\mathbf{j}_\mathrm{h} = \sum_{i=0}^{M} h_i \mathbf{j}_i$. We have $\partial_t e = \sum_{i=0}^{M} h_i \partial n_i + c\partial_t T$, where $c = T\partial s/\partial T$ is the specific heat per volume. From Equation 15, we then obtain the evolution equation for temperature,

$$c\partial_t T + \nabla \cdot \mathbf{j}_\mathrm{q} = -\sum_{i=0}^{M} \mathbf{j}_i \cdot \nabla h_i - \sum_{\alpha=1}^{R} r_\alpha \Delta h_\alpha, \tag{16.}$$

where $\Delta h_\alpha = -\sum_{i=0}^{M} \sigma_{i\alpha} h_i$ is the reaction enthalpy. The right-hand side of Equation 16 is the heat production rate per volume. The heat flux contributes to entropy flux, which reads as $\mathbf{j}_\mathrm{s} = \sum_{i=0}^{M} s_i \mathbf{j}_i + \mathbf{j}_\mathrm{q}/T$. We can finally write the entropy balance,

$$\partial_t s + \nabla \cdot \mathbf{j}_\mathrm{s} = \dot{\theta}, \tag{17.}$$

with the rate of entropy production per volume given by Equation 10. The second law of thermodynamics requires $\dot{\theta} \geq 0$.

2.5. Thin Interface Model and Kinetics of Active Emulsions

When droplets have been nucleated, the dynamics of the emulsion can be simplified when the emergent dynamics at long length scales and timescales is considered (**Figure 3*a***). If droplets are large compared to the interface width, a sharp interface limit can be employed. In the presence of chemical reactions that are maintained away from equilibrium, there are in general concentration gradients inside and outside of the droplets with position-dependent reaction fluxes (**Figure 3*b*,*c***). However, when droplets are small compared to the reaction-diffusing length scales, the droplet interior can be considered to be homogeneous. In the following, we discuss this case using a thin interface model. To this end, we consider $\beta = 1, \ldots, N$ droplets with radii R_β located at positions $\mathbf{x}_\beta$. The volume fraction fields $\phi_k(\mathbf{x}) = \nu_k n_k(\mathbf{x})$ can be considered as continuous with sources and sinks at the droplet positions. We introduce reference volume fractions $\bar{\phi}_i(t)$ that are in general time dependent and write $\phi_i(\mathbf{x}, t) = \bar{\phi}_i(t) + \psi_i(\mathbf{x}, t)$ for $i = 1, \ldots, M$. To linear order in ψ_i, the

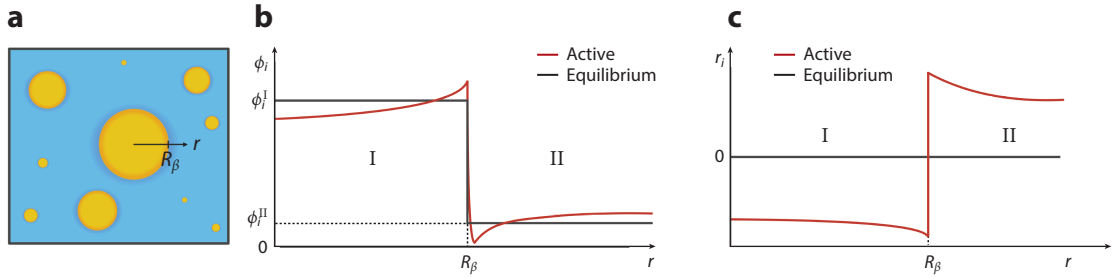

Figure 3

Chemically active emulsion. (*a*) An active emulsion is a phase-separated mixture that is composed of droplets that coexist with a surrounding phase of different composition. In both phases, chemical reactions occur that are driven away from equilibrium. (*b*) This driving can give rise to concentration gradients in each phase, which are created by diffusive fluxes and (*c*) reaction fluxes that can vary in space (*red lines* in panels *b* and *c*). Such fluxes only vanish at thermodynamic equilibrium, leading to homogeneous concentrations in each phase (*black lines* in panels *b* and *c*).

dynamic equations read

$$\partial_t \psi_i = \sum_{j=1}^{M} (\nabla \cdot D_{ij} \nabla \psi_j + A_{ij} \psi_j) - \sum_{\beta=1}^{N} s_{i\beta}\, \delta(\mathbf{x} - \mathbf{x}_\beta) - \frac{\mathrm{d}\bar{\phi}_i}{\mathrm{d}t} + B_i. \qquad 18.$$

For simplicity, we consider here the case in which the solvent does not undergo chemical reactions. Here, $D_{ij} = \nu_i \hat{D}_{ij}/\nu_j$ is the diffusion matrix, $A_{ij} = -\nu_i \sum_\alpha \sigma_{i\alpha} \partial r_\alpha / \partial \phi_j$ denotes the reaction rate matrix and $B_i = -\nu_i \sum_\alpha \sigma_{i\alpha} r_\alpha$, where $\hat{D}_{ij}$, r_α, and its derivative are evaluated at the reference composition $\bar{\phi}_i$. For a growing droplet, $s_{i\beta}$ is the volume fraction rate entering droplet β via component i. It is related to diffusion currents as

$$s_{i\beta} = \frac{2}{3} R_\beta^3 \sum_{j=1}^{M} \nabla \cdot D_{ij} \nabla \phi_j |_{\mathbf{x}=\mathbf{x}_\beta}. \qquad 19.$$

We choose the reference volume fractions as the equilibrium concentrations of macroscopic phase equilibrium $\bar{\phi}_i = \phi_{i,0}^{\mathrm{II}}$ and $\bar{\phi}_i^{\mathrm{I}} = \phi_{0,i}^{\mathrm{I}}$. These equilibrium concentrations lie on the $(M-1)$-dimensional binodal manifold that describes two-phase coexistence across a flat interface in the M-dimensional phase diagram. The dimensionality $(M-1)$ of the binodal manifold results from the Gibbs phase rule: The coexisting volume fractions $\phi_i^{\mathrm{I,II}}$ are $2M$ variables, and phase coexistence provides $(M+1)$ conditions on these variables (M conditions $\bar{\mu}_k^{\mathrm{I}} = \bar{\mu}_k^{\mathrm{II}}$ and the condition of equal pressure $p^{\mathrm{I}} = p^{\mathrm{II}}$).

The volume growth rate associated with component $i = 1, \ldots, M$ obeys the balance equation,

$$\frac{\mathrm{d}}{\mathrm{d}t}\left[\frac{4}{3}\pi R_\beta^3 (\bar{\phi}_i^{\mathrm{I}} + \psi_i^{\mathrm{I}})\right] = s_{i\beta} + \frac{4}{3}\pi R_\beta^3 \left(\sum_{j=1}^{M} A_{ij}^{\mathrm{I}} \psi_j^{\mathrm{I}} + B_i^{\mathrm{I}}\right), \qquad 20.$$

where $A_{ij}^{\mathrm{I}} = -\nu_i \sum_\alpha \sigma_{i\alpha} \partial r_\alpha / \partial \phi_j$ and $B_i^{\mathrm{I}} = -\nu_i \sum_\alpha \sigma_{i\alpha} r_\alpha$ inside droplet β, where $\phi_i^{\mathrm{I}} = \bar{\phi}_i^{\mathrm{I}} + \psi_i^{\mathrm{I}}$. Boundary conditions on the droplet surface fix $\psi_i(\mathbf{x}_\beta, t) = \phi_{i,0}^{\mathrm{II}} \ell_i^{\mathrm{II}} / R_\beta$ and $\psi_i^{\mathrm{I}} = \phi_{i,0}^{\mathrm{I}} \ell_i^{\mathrm{I}} / R_\beta$, where $\ell_i^{\mathrm{I,II}}$ are capillary lengths.

Note that the droplet growth rate $\dot{R}_\beta$ is the same for all components i. Therefore, when the rates $s_{i\beta}$ are given, the M balance (Equation 20) determines the growth rate $\dot{R}_\beta$ together with the tie-line of phase coexistence at the droplet interface on the $(M-1)$-dimensional binodal manifold (28). This fixes the coexisting volume fractions inside and outside the droplet ϕ_i^{I} and ϕ_i^{II} that serve as

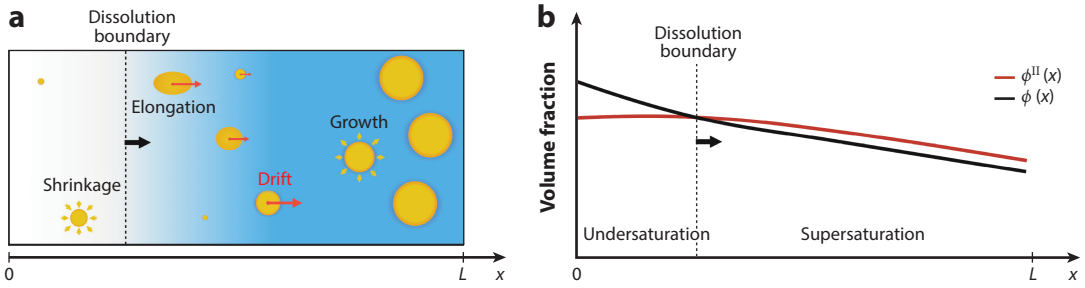

Figure 4

Overview of phenomena in emulsions with concentration gradients. (*a*) Concentration gradients in emulsions can be actively created by chemical reactions or boundary conditions and give rise to a variety of phenomena (13, 96). Droplets grow and shrink depending on position. There is a boundary that separates spatial domains of supersaturation and undersaturation (*b*), and thereby domains where droplets grow or shrink and eventually dissolve. This boundary propagates toward domains of higher supersaturation. Furthermore, droplets can drift and elongate in concentration gradients. Growing droplets in the supersaturated domains are supplied by dissolving droplets from the undersaturated regimes, leading to a transient arrest of ripening because droplets become of similar size.

reference. These equations are complemented by dynamic equations for the droplet positions,

$$\dot{\mathbf{x}}_\beta = \sum_i^M \alpha_i \nabla \phi_i|_{\mathbf{x}=\mathbf{x}_\beta}, \qquad 21.$$

where the phenomenological coefficients α_i describe droplet motion by diffusiophoresis. Diffusiophoresis can result from surface interactions of diffusing molecules such that the coefficients α_i depend on molecular details (94). For droplets in emulsions, this transport coefficient can also result from differential growth at the interface. The drift in Equation 21 results from contributions from all M components in the mixture. It therefore also describes effects of prescribed regulator gradients leading to a position-dependent supersaturation as studied in References 13, 37, and 95.

In a concentration gradient, a variety of phenomena can occur (13, 37, 95). Droplets can grow or shrink and eventually dissolve depending on position. In supersaturated domains droplets grow, whereas they shrink in undersaturated domains. The boundary between both domains moves toward domains with more supersaturation. Furthermore, droplet growth and shrinkage can also occur at opposite sides of a droplet, leading to net motion without volume growth. A droplet in concentration gradient can also elongate, and ripening can arrest transiently (see **Figure 4*a*,*b***).

The framework outlined above provides a coarse-grained simplified description of active emulsions for situations in which droplets are small compared to the reaction-diffusion length scales in the bulk. It can, for example, be applied to P granule dynamics in concentration gradients in the presence of chemical reactions.

3. PROTEIN CONDENSATES AS SOFT LIQUID MATERIALS

3.1. Single-Molecule and Collective Dynamics

For the study of biochemical processes in phase-separated droplets or in condensates in cells, understanding the dynamics of individual molecules moving in and out, typically in a diffusive process, is key. Such molecular motion can be observed in single-molecule experiments in which individual molecules are labeled and tracked and the statistics of molecular trajectories is reported (19–21). This raises the question of what is the dynamic equation that governs stochastic single-molecule motion, given the dynamics of concentration fields of a phase separating system.

One approach is to introduce the labeled molecules as a separate species at low concentration but with the same physical and chemical properties as the unlabeled one (21, 97).

To illustrate the idea, we consider an incompressible binary system with a solute concentration n of molecular volume ν with volume fraction $\phi = n\nu$ and a solvent of volume fraction $\phi_s = \nu_s n_s$ with $\phi_s = 1 - \phi$. We introduce labeled (1) and unlabeled (2) components with $\phi = \phi_1 + \phi_2$. A simple model is given by the Flory–Huggins free energy $F = \int \mathrm{d}V(f + \kappa\nu_s^{-1}(\nabla\phi)^2/2)$ with

$$f(\phi_1, \phi_2) = k_B T \left[\frac{\phi_1}{\nu} \ln \phi_1 + \frac{\phi_2}{\nu} \ln \phi_2 + \frac{1-\phi}{\nu_s} \ln(1-\phi) + \frac{\chi}{\nu_s}(1-\phi)\phi \right]. \quad 22.$$

The exchange chemical potentials $\bar{\mu}_i = \nu\delta F/\delta\phi_i$ then read as

$$\bar{\mu}_i = k_B T \left(\ln \phi_i - \frac{\nu}{\nu_s}[\ln(1-\phi) + \chi(1-2\phi)] \right) - \frac{\nu}{\nu_s}\kappa\Delta\phi. \quad 23.$$

Each volume fraction satisfies a conservation law, $\partial_t\phi_i + \nabla\cdot\mathbf{J}_i = 0$, with $\mathbf{J}_i = \nu\mathbf{j}_i$, and $\mathbf{j}_i$ is the diffusive flux. From Equation 11, we write $\mathbf{J}_i = -\sum_j M_{ij}\nabla\bar{\mu}_j$, where $M_{ij} = \nu_i\Lambda_{ij}$. We use $M_{12} = M_{21} = -m\phi_1\phi_2$ and $M_{ii} = m_s\phi_i(1-\phi) + m\phi_1\phi_2$. Here, m is a mobility describing molecular neighbor exchanges of labeled with unlabeled solute molecules, m_s describes exchanges of solutes with solvent. The probabilities for such exchanges are characterized by the ϕ_i and ϕ dependence of M_{ij}. With these definitions, the total solute volume fraction flux $\mathbf{J} = \mathbf{J_1} + \mathbf{J}_2$ reads as

$$\mathbf{J} = -D_{\mathrm{col}}\nabla\phi + m_s\frac{\nu}{\nu_s}\phi(1-\phi)\kappa\nabla\Delta\phi, \quad 24.$$

where the collective diffusion coefficient of solute in solvent is given by

$$D_{\mathrm{col}} = k_B T m_s \left[1 - 2\frac{\nu}{\nu_s}\phi(1-\phi)\chi + \phi\left(\frac{\nu}{\nu_s} - 1\right)\right]. \quad 25.$$

Note that $D_{\mathrm{col}} > 0$ if the solution is locally stable but can become negative at the spinodal line. Using this expression for $\mathbf{J}$, we can then express the currents as

$$\mathbf{J}_i = -D\left(\nabla\phi_i - \phi_i\frac{\nabla\phi}{\phi}\right) + \frac{\phi_i}{\phi}\mathbf{J}, \quad 26.$$

where $D = k_B T(m_s(1-\phi) + m\phi)$ is a self or tracer diffusion coefficient for labeled or unlabeled molecules that is always positive. The flux can also be written as a sum of diffusion and drift contributions $\mathbf{J}_i = -D\nabla\phi_i + \mathbf{v}_d\phi_i$, with drift velocity $\mathbf{v}_d = D\nabla\ln\phi + \mathbf{J}/\phi$. Note that Equation 26 has a simple form because both types of solute, (1) and (2), have the same physical properties. Introducing the effective potential $W(\mathbf{x}) = -k_B T\ln\phi(\mathbf{x})$, we have

$$\mathbf{v}_d = -(D/k_B T)\nabla W + \mathbf{v}, \quad 27.$$

with $\mathbf{v} = \mathbf{J}/\phi$. When there are only a few labeled molecules, we can interpret $\mathcal{P}(\mathbf{x},t) = \phi_1(\mathbf{x},t)/\int d^3x\,\phi_1(\mathbf{x},t)$ as the probability to find a molecule at time t at position $\mathbf{x}$. This probability then satisfies a Fokker–Planck equation,

$$\partial_t\mathcal{P} = -\nabla\cdot\mathbf{J}_\mathcal{P}, \quad 28.$$

$$\mathbf{J}_\mathcal{P} = -D\nabla\mathcal{P} - (D/k_D T)(\nabla W)\mathcal{P} + \mathbf{v}\mathcal{P}. \quad 29.$$

We can also write a Langevin equation for stochastic trajectories $\mathbf{X}(t)$ of single molecules,

$$\frac{\mathrm{d}\mathbf{X}}{\mathrm{d}t} = -\frac{D}{k_D T}\nabla W + \mathbf{v} + \nabla D + \sqrt{2D}\boldsymbol{\eta}(t), \quad 30.$$

where $\boldsymbol{\eta}(t)$ is a Gaussian white noise with $\langle \eta_i(t) \rangle = 0$ and $\langle \eta_i(t)\eta_j(t') \rangle = \delta_{ij}\delta(t - t')$. Because the diffusion coefficient D is a function of ϕ, the noise is multiplicative and the term ∇D compensates a spurious noise-induced drift. Equation 30 expresses trajectories in Ito interpretation. When the overall density profile ϕ is in equilibrium, it can exhibit an interface between coexisting phases. In an infinite system with interface perpendicular to the x axis positioned at $x = 0$, the equilibrium profile varies from ϕ^{I} (dense phase) to ϕ^{II} as

$$\phi(x) \simeq \phi^{\mathrm{II}} \left(1 + \frac{P-1}{2} [1 - \tanh(x/w)] \right), \qquad 31.$$

where $P = \phi^{\mathrm{I}}/\phi^{\mathrm{II}}$ is the partition coefficient and $w \simeq (k_{\mathrm{B}}T/\kappa)^{1/2}$ is the interface width. In this case, $\mathbf{J} = 0, \mathbf{v} = 0$ and the probability reaches a Boltzmann distribution $\mathcal{P}^{\mathrm{eq}} = \exp(-W/k_{\mathrm{B}}T)$. Molecules feel an effective potential with a steep jump over $\Delta W = W^{\mathrm{II}} - W^{\mathrm{I}} = k_{\mathrm{B}}T \ln P$.

When in a homogeneous phase, a concentration gradient $\nabla\phi$ is imposed; this generates a flux $\mathbf{J} \simeq -D_{\mathrm{col}}\nabla\phi$ and a drift velocity of single molecules $v_{\mathrm{d}} \simeq (D - D_{\mathrm{col}})\nabla\phi/\phi$, where we have neglected the contribution $\sim\kappa\nabla\Delta\phi$. We can also write this as

$$\mathbf{v}_{\mathrm{d}} \simeq \left(1 - \frac{D}{D_{\mathrm{col}}} \right) \frac{\mathbf{J}}{\phi}. \qquad 32.$$

Interestingly, for $D_{\mathrm{col}} < D$ the single-molecule drift is in the opposite direction as that of the net diffusive flux $\mathbf{J}$ (**Figure 5**). Using the definitions of D and D_{col}, we have

$$\mathbf{v}_{\mathrm{d}} \simeq \frac{\nu/\nu_{\mathrm{s}} - m/m_{\mathrm{s}} - 2\chi(\nu/\nu_{\mathrm{s}})(1-\phi)}{1 + \phi[(\nu/\nu_{\mathrm{s}} - 1) - 2\chi(\nu/\nu_{\mathrm{s}})(1-\phi)]} \mathbf{J}. \qquad 33.$$

Note that in the absence of interactions, single-molecule trajectories do not exhibit drift even in the presence of a concentration gradient that leads to a diffusion flux. This corresponds to the case $\nu = \nu_{\mathrm{s}}$, $m = m_{\mathrm{s}}$, and $\chi = 0$ in Equation 33. Diffusion fluxes arise as an ensemble effect, but single-molecule trajectories do not exhibit net transport, $\mathbf{v}_{\mathrm{d}} = 0$. However, in crowded systems that may also phase-separate molecular interactions and collective effects are important. This leads to a net drift of individual diffusing molecules in the presence of concentration gradients within a phase. This collective behavior is therefore fundamentally different from simple diffusion of noninteracting molecules.

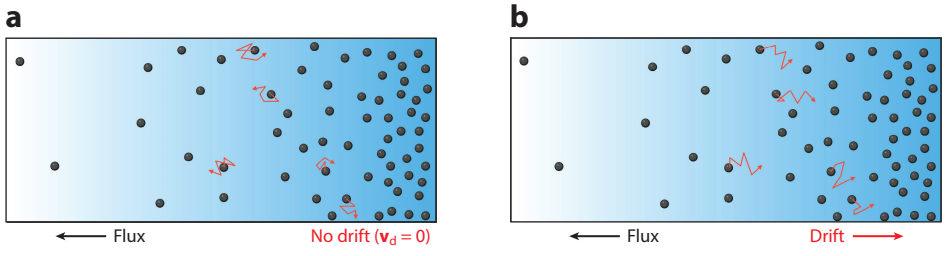

Figure 5

Sketch of molecular diffusion and drift in a concentration gradient. (*a*) Stochastic trajectories of individual molecules that are independent and noninteracting are unbiased and have no net drift $\mathbf{v}_{\mathrm{d}}$, even in the presence of a concentration gradient that leads to a net diffusion flux. (*b*) If molecules interact, stochastic trajectories of individual molecules can exhibit a nonvanishing drift, $\mathbf{v}_{\mathrm{d}}$, if a concentration gradient is imposed. This drift can be parallel or antiparallel to the collective diffusive flux (see Equation 33). The drift of individual molecules in a gradient stems from interactions among molecules that are also relevant for phase separation. Note that if the drift of the stochastic trajectories is antiparallel with respect to the net diffusive flux, the drift of individual molecules is uphill with respect to the concentration gradient.

Single-molecule trajectories in biological condensates can be observed experimentally. Recently, stochastic trajectories of RNA polymerase entering and leaving viral replication compartments have been observed (19). The authors found that the step size distributions of molecules moving into a condensate or leaving the condensate were the same. This is consistent with a passive diffusive process across an interface separating two coexisting phases. Note that the authors of Reference 19 interpreted their results differently, claiming that these statistics suggest a different physical process. However, our analysis (97) shows that the data in Reference 19 provide evidence for passive motion of RNA polymerase into a phase-separated compartment.

3.2. Rheology of Protein Condensates

Protein condensates often have liquid-like properties. They take a spherical shape, they undergo fusion (9, 22), and their component molecules exhibit rapid diffusion (9, 20, 21). However, proteins and RNA are complex polymeric macromolecules. Such molecules form a complex soft material when condensing in a phase. Therefore, biological condensates can have rich and variable material properties. Liquid-like condensates are often highly dynamic and enable rapid exchange of molecular components via diffusion and mass action chemical kinetics. Because of the polymeric nature of the components, transient entanglements or cross-links can lead to viscoelastic response to mechanical stimulation (75). Because of the small volumes of condensate droplets, microrheology can be employed to study the rheology of these systems. A key example is the use of optical tweezers to act on small beads attached to a mesoscopic droplet (98, 99). This active microrheology technique permits measuring the surface tension of droplets but also the frequency-dependent complex modulus $G^*(\omega)$ describing the stress in response to a time-periodic strain at angular frequency ω. Here, the complex modulus is the Fourier transform of the time-dependent modulus $G(t)$

$$G^*(\omega) = \int_0^\infty \mathrm{d}t\, G(t) e^{i\omega t}, \qquad 34.$$

where $G(t) = 0$ for $t < 0$ because of causality. Such experiments reveal a surface tension of protein droplets on the order of a few micronewtons per meter. In Reference 99, the authors show that the complex modulus can be well described by a simple Maxwell model with a single relaxation time τ as $G^*(\omega) = i\omega\tau E/(1 + i\omega\tau)$, where E is the short-time elastic modulus and $\eta = \tau E$ is the long-time viscosity. Such active microrheology directly measures the mechanical response. Alternatively, passive microrheology can be employed in which the spontaneous stochastic movements of an immersed bead are quantified. Because of the fluctuation–dissipation relation, the time-dependent mean square displacement $\langle \Delta r^2 \rangle(t) = \langle (r(t) - r(0))^2 \rangle$ can be related to the complex modulus obtained by active microrheology:

$$\tilde{G}(s) = \frac{d k_\mathrm{B} T}{3\pi a s \langle \Delta r^2 \rangle(s)}, \qquad 35.$$

where $\tilde{G}(s) = G^*(\omega = is)$ is the Laplace transform of the time-dependent modulus, and $\langle \Delta r^2 \rangle(s)$ denotes the Laplace transform of $\langle \Delta r^2 \rangle(t)$.

An interesting phenomenon that is often observed in droplets of purified proteins is that the dynamics of droplets slows after preparation and that material properties depend on age (100). This ageing phenomenon has been studied quantitatively, suggesting that such ageing condensates have glassy material properties (99). Interestingly, the ageing could be characterized simply by an age-dependent relaxation time $\tau(t_\mathrm{w})$, and the glassy rheology of the condensates could be well captured by the age-dependent complex modulus

$$G^*(\omega, t_\mathrm{w}) = \frac{i\omega\tau(t_\mathrm{w})E}{(1 + i\omega\tau(t_\mathrm{w}))}, \qquad 36.$$

whereas the elastic modulus E remained essentially unchanged. Here, t_w denotes the waiting time after preparation of the sample before a microrheology measurement was performed.

The liquid-like nature of biological condensates is important to spatially organize chemical processes. Glassy material properties slow down chemical rates and could be used by a cell to create a dormant state to protect molecules (101, 102). The fact that protein droplets in vitro often exhibit glassy dynamics and ageing raises the question of how cells control the material properties of biomolecular condensates. Some degenerative diseases are in fact associated with the formation of stable aggregates of proteins that can form droplets in vitro and organize condensates in vivo (103). To understand how cells maintain the liquid state of many condensates and how this fails in some diseases remains a challenging question for the future.

4. PROTEIN CONDENSATES AT SURFACES

Phase-separated liquid droplets in the bulk are known to interact with surfaces (104–108). Droplets can partially wet a surface and establish at the triple line a contact angle between the droplet and surface. This angle is set by the interaction among all three phases touching at the triple line: the dense droplet phase, the dilute outside phase and the surface. The corresponding relationship is referred to as Young-Dupré law, $\gamma_{s,\alpha} = \gamma_{s,\beta} + \gamma_{\alpha,\beta}\cos(\theta)$, where $\gamma_{\alpha\beta}$ are the respective interaction-specific surface tensions among surface (s), dilute (α), and dense (β) phase. For increasing adhesive interactions with the surface, the wetting angle decreases toward zero. Upon passing the threshold $\gamma_\beta = \gamma_{s,\beta} + \gamma_{\alpha,\beta}$, a wetting transition occurs in which a partially wet droplet transitions to a completely wetted layer. There can also be a phase transition below the saturation concentration above which coexisting phases such as droplets can form in the bulk; it is referred to as the prewetting phase transition (104, 106). It was an experimental challenge to confirm Cahn's prediction of prewetting phase transitions (104) because the first-order prewetting transition line is close to the saturation concentration in experimental polymeric systems (109, 110).

The observation in living cells that droplet-like biomolecular condensates can wet membrane bound organelles such as the nucleus (9, 111), intracellular filaments (112), and the cell membrane (64) suggests that the physics of wetting plays a crucial role for the intracellular organization in living cells. Reference 113 critiques equilibrium explanations of lipid organization and argues that the membrane of the living cell is an active composite. However, in living cells, phase separating proteins can also specifically bind to receptor molecules embedded in the membrane surface (67) or sequence motifs along biopolymers (68). The ability of binding naturally enhances the possibility of surface phase transitions (65); i.e., when molecules are bound to a surface they can utilize phase separation in the two-dimensional surface or along a one-dimensional filament. The interplay of surface phase transitions and wetting suggests a rich number of phases when drops can get in contact with biological surfaces (see **Figure 6** for an overview). Recent experiments using lipid bilayers show evidence for rich behavior due to this interplay (114–116). In living cells, droplet wetting was shown to, for example, mediate cleaning of cellular waste (117).

4.1. Wetting, Prewetting, and Surface Phase Separation on Membranes

To illustrate the role of surface binding on wetting transitions, we consider a minimal model at thermodynamic equilibrium (65) in which solute molecules can bind to specific sites on a two-dimensional, flat membrane at $z = 0$. This system is homogeneous parallel to the membrane, i.e., effectively one-dimensional with a bulk volume fraction $\phi(z)$ changing along the z-direction with $z \in [0, \infty)$. During binding and unbinding events, molecules transition between the solute state and the surface bound state according to $\phi \rightleftharpoons \phi_m$. The interaction between the different states can

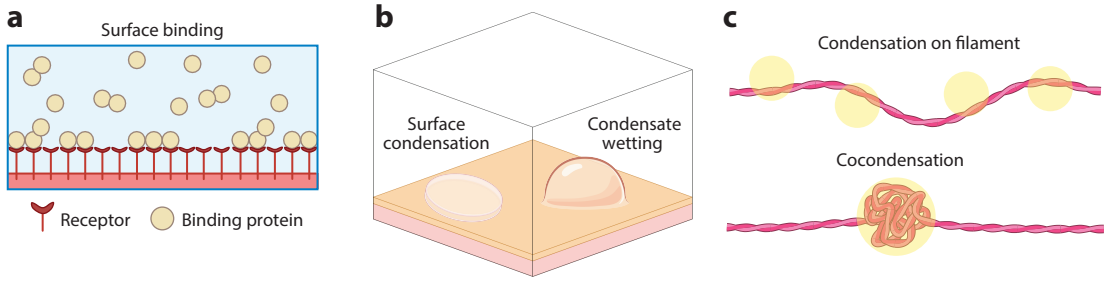

Figure 6

Phase transitions at biological surfaces. (*a*) Biomolecules can bind to surfaces such as membranes often by attaching to specific receptors. (*b*) Binding can facilitate wetting of bulk condensates and can also lead to surface-related phase transitions below the bulk saturation concentration such as prewetting and surface phase separation. (*c*) Below bulk saturation, condensation can also occur on a filament or polymer. Alternatively, a polymer can form a condensed phase together with a phase separating protein. This cocondensation can also give rise to capillary forces acting on the polymer.

be described by a free energy that contains contributions from the bulk $f_b(\phi)$ and the membrane $f_m(\phi_m)$ and coupling free energy between them, $J(\phi|_0, \phi_m)$:

$$f_s[\phi, \phi_m] = \int_0^\infty dz \left[f_b(\phi) - f_b(\phi_\infty) + \frac{1}{2}\kappa |\partial_z \phi|^2 \right] + f_m(\phi_m) + J(\phi|_0, \phi_m), \quad 37.$$

where $\phi_\infty = \phi(z \to \infty)$ with the corresponding external chemical potential $\mu_\infty = df_b/d\phi|_{\phi=\phi_\infty}$. The thermodynamic order parameter for the wetting phase transitions is excess surface concentration

$$c_s = \int_0^\infty dz \left[\frac{1}{\nu_b} (\phi(z) - \phi_\infty) \right]. \quad 38.$$

The surface free energy $f_s(c_s, \phi_m)$ is obtained when evaluating f_s for the profile $\phi(z)$ that minimizes Equation 37 for fixed c_s and ϕ_m, and with ϕ_∞ given far away from the membrane. The surface free energy $f_s(c_s, \phi_m)$ depends on the membrane area fraction ϕ_m and the excess surface concentration c_s and has units of an energy per area. The chemical potentials in bulk and membrane can now be expressed as $\mu = \partial f_s/\partial c_s$ and $\mu_m = \nu_m \partial f_s/\partial \phi_m$. The Gibbs surface free energy $\gamma_s(\mu, \mu_m)$ corresponds to the surface thermodynamic potential in the ensemble where the chemical potentials are fixed and can be obtained via a Legendre transformation,

$$\gamma_s(\mu, \mu_m) = f_s(c_s, \phi_m) - \mu c_s - \mu_s \frac{\phi_s}{\nu_s}. \quad 39.$$

The conjugate variables to each of the chemical potentials μ and μ_m are the excess surface concentration $c_s = -\partial\gamma_s/\partial\mu$ and the area fraction $\phi_m = -\nu_m \partial\gamma_s/\partial\mu_m$. Both variables serve as order parameters for wetting, prewetting, and surface phase transitions. In particular, c_s characterizes the bulk layer adjacent to the surface, whereas ϕ_m describes the state of the membrane.

The transition lines separating different thermodynamic states at the surface can be obtained via a graphical Maxwell construction. The Gibbs surface free energy functional can be expressed as (for details, see Reference 65):

$$\gamma(\phi, \phi_\infty) = \int_{\phi_\infty}^{\phi} d\phi' \left[\pm \sqrt{2\kappa W(\phi')} + \frac{\partial J_m}{\partial \phi'} \right] + J_m(\phi_\infty), \quad 40.$$

where $J_m(\phi) = \hat{J}(\phi, \hat{\phi}_m)$, and $\hat{J}(\phi, \phi_m) = J(\phi, \phi_m) + f_m(\phi_m) - \nu_m^{-1}\mu_\infty \phi_m$ with $\hat{\phi}_m$ satisfying $\partial\hat{J}/\partial\phi_m = 0$. The integral term in Equation 40 corresponds to the area between $\pm\sqrt{2\kappa W(\phi)}$ and $-\partial J_m/\partial\phi$ and can be illustrated graphically (see Reference 65 for an illustration).

Now we can define the Gibbs surface potential as $\gamma_s = \gamma(\phi|_0, \phi_\infty)$. Local extrema of the Gibbs surface potential correspond to the intersection points between $\pm\sqrt{2\kappa W(\phi)}$ and $-\partial J_m/\partial\phi$. There can be two local minima, $\gamma_\alpha = \gamma_s(\phi|_{0,\alpha}, \phi_\infty)$ and $\gamma_\beta = \gamma_s(\phi|_{0,\beta}, \phi_\infty)$, and the intermediate local maximum is denoted by $\gamma_u = \gamma_s(\phi|_{0,u}, \phi_\infty)$. The differences between these extremal values of the Gibbs surface potential can be expressed as the areas between $\pm\sqrt{2\kappa W(\phi)}$ and $-\partial J_m/\partial\phi$. Specifically, $\gamma_\alpha = -S_0 + J_m(\phi_\infty)$, $\gamma_u = -S_0 + S_1 + J_m(\phi_\infty)$, and $\gamma_\beta = -S_0 + S_1 - S_2 + J_m(\phi_\infty)$. Thus, we find that the surface free energies at the minima are related by $\gamma_\alpha = \gamma_\beta + S_1 - S_2$.

At the prewetting and wetting transition lines, the Gibbs surface free energies of both states α and β are equal, $\gamma_\alpha = \gamma_\beta$, which implies that $S_1 = S_2$ at the transition line. This defines the graphical construction and determines the value of the control parameter, e.g., $\bar{\phi}$, at which the transition occurs. The minimized surface free energies exhibit a kink at both the wetting and prewetting transitions (characterized by c_s) and the surface phase transition (characterized by ϕ_m). However, due to the coupling between bulk and membrane, both order parameters, area fraction ϕ_m and the excess surface concentration c_s, in general change discontinuously at each of the transitions.

If the average volume fraction of the system $\bar{\phi}$ is within the domain of phase coexistence, i.e., $\phi_\alpha < \bar{\phi} < \phi_\beta$ for a certain range of interaction parameters, the homogeneous mixture is unstable and phase-separates into a dilute and a dense phase, with respective equilibrium values ϕ_α and ϕ_β. Based on the definition of the Gibbs surface free energy density $\gamma_s = \gamma(\phi|_0, \phi_\infty)$ (Equation 40), we identify the surface tensions between the membrane and the dilute phase $\gamma_{s,\alpha}$, between the membrane and the dense phase $\gamma_{s,\beta}$, and between the dilute and dense phases $\gamma_{\alpha,\beta}$, as follows:

$$\gamma_{s,\alpha} = \gamma(\phi|_{0,\alpha}, \phi_\alpha), \quad \gamma_{s,\beta} = \gamma(\phi|_{0,\beta}, \phi_\beta), \quad \gamma_{\alpha,\beta} = \int_{\phi_\alpha}^{\phi_\beta} \mathrm{d}\phi\, \sqrt{2\kappa W}. \tag{41.}$$

These surface tensions determine the contact angle via Young–Dupré law, $\gamma_{s,\alpha} = \gamma_{s,\beta} + \gamma_{\alpha,\beta}\cos(\theta)$, which defines the contact angle. The wetting transition is characterized by equal Gibbs surface free energy of the partially wetted state $\gamma_\alpha = \gamma_{s,\alpha}$ and the completely wetted state $\gamma_\beta = \gamma_{s,\beta} + \gamma_{\alpha,\beta}$, corresponding to zero contact angle, $\theta = 0$.

If the average volume fraction of the system $\bar{\phi}$ is outside the domain of phase coexistence, e.g., $\bar{\phi} < \phi_\alpha$ or $\bar{\phi} > \phi_\beta$, there can still be two surface states corresponding to two local minima of the Gibbs surface free energy. When these free energies are equal ($\gamma_\alpha = \gamma_\beta$), a phase transition occurs. Due to the coupling between bulk and membrane, the corresponding phase transition in general shares the characteristics of a prewetting transition with a discontinuous behavior in the excess surface concentration c_s and a surface phase transition with discontinuous behavior of the membrane area fraction ϕ_m.

Despite the minimal nature of the considered model, the ability of membrane binding can lead to a variety of thermodynamic surface states at undersaturated conditions with unexpectedly rich surface phase diagrams (see **Figure 6** and Reference 65 for an overview). Such states are characterized by the order parameters c_s and ϕ_m. There are even cases in which phase transitions at and adjacent to surfaces occur at conditions such that the bulk cannot phase-separate for any concentration. More generally, a layer of bound molecules on the membrane effectively modifies the properties of the surface, which can, for example, lead to a shift of the prewetting line to low concentrations, thereby deviating from the saturation concentration by an order of magnitude. This finding suggests that the physics of prewetting phase transition with molecular binding provides a versatile and robust mechanism to control the position of wetted droplets.

4.2. Condensation and Cocondensation on Biopolymers

Wetting of condensates occurs on not only flat surfaces such as membranes but also the surface of filaments or biopolymers. The first example of such phenomena was observed for the microtubule

associated protein Tau, which binds to microtubules (118). Tau also forms droplets in vitro that interact with microtubules. It was shown that Tau condensates in vitro deform in the presence of microtubules. Wetting on microtubules leads to bundling by capillary effects that appear to correspond to complete wetting. Another microtubule-associated protein, TPX2, forms droplets that also wet microtubules. The wetting layer on the microtubule surface breaks up into separate droplets due to a Rayleigh–Plateau instability as an example of wetting on a cylinder surface (119, 120). Condensates formed by microtubule-associated proteins can have important implications for microtubule organization in the cell and for disease (119, 121, 122).

Another situation in which protein that can form condensates binds to polymers is the case of transcription factors binding to DNA to regulate gene expression. The pioneer transcription factor Klf4 can form droplets in buffer solution at concentrations above 1 μM. This saturation is higher than concentrations in the cell nucleus. However, in the presence of DNA that is stretched by an external force, Klf4 forms small assemblies at much lower concentrations (68). These assemblies can be interpreted as a result of a prewetting transition on a heterogeneous polymer surface. At very low protein concentrations, small numbers of largely individual molecules bind preferentially to certain sequences. As the protein concentration is increased, suddenly larger assemblies containing hundreds to about a thousand molecules form. This transition to condensate formation is similar to a prewetting transition on a planar surface. However, because of the sequence dependence of protein binding, this prewetting only occurs in regions along DNA where patterns of a sequence-binding motif that facilitate Klf4 binding occur. The transition to form Klf4-rich condensates on DNA by prewetting is a collective behavior that emerges from many molecules along a longer stretch of DNA and is therefore fundamentally different from sequence-specific binding of single molecules to DNA.

Transcription factors can also form protein–DNA cocondensates. In this case, DNA is not fully stretched and the condensate that forms contains both DNA and proteins (69, 70). A simple model for the cocondensation of double-stranded DNA with protein is based on the droplet free energy of the condensate together with the free energy of stretching of the DNA that remains outside the condensate. Denoting L as the distance between the endpoints of the DNA and L_c as the DNA contour length, the free energy of a cocondensate containing contour length L_d can be written as

$$F(L, L_d) = -\Delta f \alpha L_d + \gamma 4\pi \left(\frac{3\alpha}{4\pi}\right)^{2/3} L_d^{2/3} + \frac{k_B T}{\ell}\left(\frac{(L_c - L_d)^2}{4(L_c - L_d - L)} - \frac{L}{4} + \frac{L^2}{2(L_c - L_d)} - \frac{L_c - L_d}{4}\right). \quad 42.$$

Here, α describes the packing density in the condensate with volume $V_d = \alpha L_d$, and Δf is the free energy gain per volume of cocondensation relative to stretched DNA and dissolved proteins in solution. Furthermore, γ denotes surface tension and the persistence length of DNA is denoted by ℓ. The first term in Equation 42 is the condensation free energy, the second term is the droplet surface free energy, and the last term describes the free energy of stretching of the noncondensed DNA.

Because of the mesoscopic size of condensates, fluctuations are relevant. The distribution of contour length L_d for fixed L is therefore given by

$$P(L_d|L) = \frac{1}{Z(L)} \exp\left(-\frac{F(L, L_d)}{k_B T}\right), \quad 43.$$

where $Z(L)$ is a partition function that normalizes the distribution. For fixed extension L, the average force generated by condensation is then given by

$$f = k_B T \frac{\mathrm{d} \log Z(L)}{\mathrm{d}L}. \quad 44.$$

This system exhibits a sharp transition between a state of stretched DNA and a condensate for L below a critical distance. In the absence of fluctuations, this transition corresponds to a first-order transition. Strikingly, there is a force dependence of condensate formation giving rise to the generation of capillary forces in DNA by condensates. It has been suggested that such capillary forces could play a key role in DNA remodeling as they are of similar size to forces generated by active molecules, for example, during DNA loop extrusion (123, 124).

5. OUTLOOK

Biological condensates with properties of phase-separated droplets in living cells are ubiquitous across almost all cells (16, 30). They provide distinct physicochemical environments to tame and control chemical reactions in living cells. As a result, cells can provide certain biological functions such as enhanced robustness against stress (26) or fluctuations (31). The formation of biological condensates as phase-separated droplets in a cell can be captured by nonequilibrium thermodynamics. The applicability of such concepts (73, 83) to reveal principles underlying important cellular processes is appealing. Revealing cellular principles is feasible because concentration profiles can be experimentally observed and theoretically determined, and fluxes of heat and matter can be calculated and finally compared with experiments. However, the complexity of living cells poses many challenges for quantitative approaches to biomolecular condensates that aim at a physical understanding of the spatial organization of biochemistry in living cells.

A fundamental challenge is related to the large number of different molecular components. Living cells contain thousands of different components such as proteins, lipids, RNA, and DNA (1, 82). This multicomponent nature of cells requires concepts to identify the relevant microscopic variables that affect the formation and function of biomolecular condensates on mesoscopic scales. Another approach is to use models with a large number of components. Recent work on the theory of multicomponent polymeric liquids used random interaction matrices and random matrix theory (126–128) or Monte Carlo simulations (129) to determine phase coexistence in multicomponent mixtures. Such approaches considered the special case of equally concentrated components. However, concentrations in living cells span over seven orders of magnitude, from 1 nM to 10 mM. In fact, a recent theoretical study showed that such random interactions typically do not lead to a precise number of phases, whereas evolutionarily optimized interactions do (130). It remains elusive how many phases can coexist in living cells given the large variety of interactions and concentration of the components (131).

A further challenge is related to the intrinsic complexity of molecules, often arising from the sequences of building blocks such as nucleotides or amino acids. It would be valuable to develop theoretical concepts for condensate formation that can account for the impact of the distribution of polymer length (e.g., RNA or DNA) and its sequence on phase separation. Such approaches would ideally describe the effects of detailed or coarse-grained sequence properties such as sequence patterns and could be compared with coarse-grained polymer models such as those involving stickers and spacers (132–135). Recent approaches made use of the random phase approximation to heteropolymers with specific sequences (77, 78). However, such approaches are not yet able to provide quantitative agreement with in vitro and in vivo phase diagrams. Such works nevertheless represent important steps toward a theory of sequence-dependent polymer phase separation. Their methods could also be very useful when incorporating sequence dependence of chemical processes and could help to bridge between the relevant microscopic degrees of freedom and the biochemical functions that arise on mesoscopic scales.

Another challenge is related to the fact that biomolecular condensates in vitro and in vivo can be heterogeneous. Various experimental studies reported cluster-like heterogeneities inside

condensates as well as outside (100, 136). Already below the saturation concentration, protein assemblies with sizes in the nanometer range could be observed (137) but also solid fibril structures can emerge (138). Notably this is the case for proteins such as FUS, which is involved in neurodegenerative diseases (103). Only a few theoretical studies address assembly formation at nondilute, i.e., crowded, conditions, where assemblies can form in a phase separating system. For example, the assembly size distributions at equilibrium are generally different in two coexisting phases and in particular the dense phase can transition to a gel (132, 139–141). Only recently, such theories were applied to the specifics of protein interactions, and extensions of this theoretical framework were used to address nonequilibrium effects (142). Comparing theoretical predictions of such works with the experimental characterization of size distributions of molecular assemblies using, for example, Förster resonance energy transfer (FRET) (143) could allow for deciphering the molecular interactions involved in the interplay between phase separation and molecular assembly. Such insights could then be used to address the pathways for how biomolecular condensates can regulate aberrant assemblies like amyloids (96, 144, 145).

Another exciting question concerns the transport through the interfaces that separate coexisting phases. Gradients in chemical potentials give rise to diffusive fluxes within the phases as well as across the interface. In many cases, the interface has a thickness on the order of molecular scales. Due to this small length scale, diffusion across the interface is often fast compared to other timescales. However, this may not be the case once the interface involves chemical reactions or energy barriers for molecule diffusion. The latter could arise, for example, when surfactants accumulate at the interface or when interfaces are charged, which was reported for biomolecular condensates (146). These effects can reduce the interface mobilities, which is an effect sometimes called interfacial friction (147, 148), giving rise to additional timescales. If these timescales are rate limiting, i.e., if they exceed other timescales in the system, such as the ones for diffusion or chemical reactions, droplet kinetics could be significantly altered. It has been proposed that individual molecules could effectively bounce back at the interface if they are capable of self-collapse into a nonsticking conformation (149). On larger scales, a reduced interface mobility could affect ripening exponents for the growth of the average radius (150). Such ways to regulate the dynamics of phase-separated systems by altering the transport properties of the interface suggest that cells may use condensate-specific surfactants or the regulation of condensate surface charge to control molecular transport and exchange with the condensate environment. A recent study in cells provides evidence that condensate growth is regulated by changing the interface permeability by small protein clusters (151) or RNA (152), a situation similar to Pickering emulsions. A selective permeability of molecules is reminiscent of membrane channels (153, 154). In other words, membraneless organelles could regulate transport at the phase boundaries similar to those found for membrane bound organelles.

In summary, addressing the complexity of biological condensates in cells using nonequilibrium physics has just begun. Many open questions remain that present exciting challenges for future work.

DISCLOSURE STATEMENT

The authors are not aware of any affiliations, memberships, funding, or financial holdings that might be perceived as affecting the objectivity of this review.

ACKNOWLEDGMENTS

We thank I. Haugerud for designing the figures and J. Bauermann, A. Fritsch, and I. Haugerud for feedback on the article. F. Jülicher acknowledges funding by the Volkswagen Foundation. C.A.

Weber acknowledges the European Research Council (ERC) under the European Union's Horizon 2020 research and innovation program ("Fuelled Life" with grant agreement 949021) for financial support. Figures were created using BioRender.

LITERATURE CITED

1. Alberts B, Bray D, Hopkin K, Johnson AD, Lewis J, et al. 2015. *Essential Cell Biology*. New York: Tayor & Francis Group
2. Hyman AA, Weber CA, Jülicher F. 2014. *Annu. Rev. Cell Dev. Biol.* 30:39–58
3. Brangwynne CP. 2013. *J. Cell Biol.* 203(6):875–81
4. Zwicker D, Decker M, Jaensch S, Hyman AA, Jülicher F. 2014. *PNAS* 111(26):E2636–45
5. Woodruff JB, Gomes BF, Widlund PO, Mahamid J, Honigmann A, Hyman AA. 2017. *Cell* 169(6):1066–77
6. Brangwynne CP, Mitchison TJ, Hyman AA. 2011. *PNAS* 108(11):4334–39
7. Feric M, Vaidya N, Harmon TS, Mitrea DM, Zhu L, et al. 2016. *Cell* 165(7):1686–97
8. Lafontaine DL, Riback JA, Bascetin R, Brangwynne CP. 2021. *Nat. Rev. Mol. Cell Biol.* 22(3):165–82
9. Brangwynne CP, Eckmann CR, Courson DS, Rybarska A, Hoege C, et al. 2009. *Science* 324(5935):1729–32
10. Updike DL, Knutson AK, Egelhofer TA, Campbell AC, Strome S. 2014. *Curr. Biol.* 24(9):970–75
11. Strome S, Wood WB. 1983. *Cell* 35:15–25
12. Lee CF, Brangwynne CP, Gharakhani J, Hyman AA, Jülicher F. 2013. *Phys. Rev. Lett.* 111(8):088101
13. Weber CA, Lee CF, Jülicher F. 2017. *New J. Phys.* 19(5):053021
14. Griffin EE, Odde DJ, Seydoux G. 2011. *Cell* 146(6):955–68
15. Schubert CM, Lin R, De Vries CJ, Plasterk RH, Priess JR. 2000. *Mol. Cell* 5(4):671–82
16. Banani SF, Lee HO, Hyman AA, Rosen MK. 2017. *Nat. Rev. Mol. Cell Biol.* 18(5):285–98
17. Alberti S. 2017. *Curr. Biol.* 27(20):R1097–102
18. Boeynaems S, Alberti S, Fawzi NL, Mittag T, Polymenidou M, et al. 2018. *Trends Cell Biol.* 28(6):420–35
19. McSwiggen DT, Hansen AS, Teves SS, Marie-Nelly H, Hao Y, et al. 2019. *eLife* 8:e47098
20. Taylor NO, Wei MT, Stone HA, Brangwynne CP. 2019. *Biophys. J.* 117(7):1285–300
21. Hubatsch L, Jawerth LM, Love C, Bauermann J, Tang TD, et al. 2021. *eLife* 10:e68620
22. Ghosh A, Kota D, Zhou HX. 2021. *Nat. Commun.* 12:5995
23. Weber CA, Zechner C. 2021. *Phys. Today* 74(6):38–43
24. Hnisz D, Shrinivas K, Young RA, Chakraborty AK, Sharp PA. 2017. *Cell* 169:13–23
25. Maharana S, Wang J, Papadopoulos DK, Richter D, Pozniakovsky A, et al. 2018. *Science* 360(6391):918–21
26. Franzmann TM, Alberti S. 2019. *Cold Spring Harb. Perspect. Biol.* 11(6):a034058
27. Nakashima KK, Vibhute MA, Spruijt E. 2019. *Front. Mol. Biosci.* 6:21
28. Bauermann J, Laha S, McCall PM, Jülicher F, Weber CA. 2022. *J. Am. Chem. Soc.* 144(42):19294–304
29. Spruijt E. 2023. *Commun. Chem.* 6:23
30. Lyon AS, Peeples WB, Rosen MK. 2021. *Nat. Rev. Mol. Cell Biol.* 22(3):215–35
31. Klosin A, Oltsch F, Harmon T, Honigmann A, Jülicher F, et al. 2020. *Science* 367(6476):464–68
32. Roden C, Gladfelter AS. 2021. *Nat. Rev. Mol. Cell Biol.* 22(3):183–95
33. Tibble RW, Depaix A, Kowalska J, Jemielity J, Gross JD. 2021. *Nat. Chem. Biol.* 17(5):615–23
34. Wunder T, Mueller-Cajar O. 2020. *Curr. Opin. Plant Biol.* 58:1–7
35. Sagui C, Grant M. 1999. *Phys. Rev. E* 59(4):4175–87
36. Bray AJ. 2002. *Adv. Phys.* 51(2):481–587
37. Weber CA, Zwicker D, Jülicher F, Lee CF. 2019. *Rep. Prog. Phys.* 82(6):064601
38. Shimobayashi SF, Ronceray P, Sanders DW, Haataja MP, Brangwynne CP. 2021. *Nature* 599(7885):503–6
39. Lomakin A, Asherie N, Benedek GB. 1996. *J. Chem. Phys.* 104(4):1646–56
40. Bartolucci G, Adame-Arana O, Zhao X, Weber CA. 2021. *Biophys. J.* 120(21):4682–97
41. Adame-Arana O, Weber CA, Zaburdaev V, Prost J, Jülicher F. 2020. *Biophys. J.* 119(8):1590–605

42. Overbeek JTG, Voorn M. 1957. *J. Cell. Comp. Physiol.* 49(S1):7–26
43. de Groot SR, Mazur P. 1984. *Non-Equilibrium Thermodynamics*. New York: Dover Publ. Unabridged, corrected republication ed.
44. Alberty RA. 2003. *Thermodynamics of Biochemical Reactions*. Hoboken, NJ: Wiley-Intersci.
45. Glotzer SC, Di Marzio EA, Muthukumar M. 1995. *Phys. Rev. Lett.* 74(11):2034–37
46. Zwicker D, Hyman AA, Jülicher F. 2015. *Phys. Rev. E* 92:012317
47. Wurtz JD, Lee CF. 2018. *Phys. Rev. Lett.* 120(7):078102
48. Zwicker D, Seyboldt R, Weber CA, Hyman AA, Jülicher F. 2017. *Nat. Phys.* 13(4):408–13
49. Seyboldt R, Jülicher F. 2018. *New J. Phys.* 20(10):105010
50. Bergmann AM, Bauermann J, Bartolucci G, Donau C, Stasi M, et al. 2023. *Nat. Commun.* 14:6552
51. Bauermann J, Weber CA, Jülicher F. 2022. *Ann. Phys.* 534(9):2200132
52. Zwicker D. 2022. *Curr. Opin. Colloid Interface Sci.* 61:101606
53. Heltberg ML, Miné-Hattab J, Taddei A, Walczak AM, Mora T. 2021. *eLife* 10:e69181
54. Bajpai G, Amiad Pavlov D, Lorber D, Volk T, Safran S. 2021. *eLife* 10:e63976
55. Zhang Y, Lee DS, Meir Y, Brangwynne CP, Wingreen NS. 2021. *Phys. Rev. Lett.* 126(25):258102
56. Adame-Arana O, Bajpai G, Safran S. 2021. *Biophys. J.* 120(3):318a–319a
57. Wei MT, Chang YC, Shimobayashi SF, Shin Y, Strom AR, Brangwynne CP. 2020. *Nat. Cell Biol.* 22(10):1187–96
58. Deviri D, Safran SA. 2021. *PNAS* 118(25):e2100099118
59. Terlecki-Zaniewicz S, Humer T, Eder T, Schmoellerl J, Heyes E, et al. 2021. *Nat. Struct. Mol. Biol.* 28(2):190–201
60. Strom AR, Emelyanov AV, Mir M, Fyodorov DV, Darzacq X, Karpen GH. 2017. *Nature* 547(7662):241–45
61. Michieletto D, Colì D, Marenduzzo D, Orlandini E. 2019. *Phys. Rev. Lett.* 123(22):228101
62. Lohse DJ, Hadjichristidis N. 1997. *Curr. Opin. Colloid Interface Sci.* 2(2):171–76
63. Clark A, Kavanagh G, Ross-Murphy S. 2001. *Food Hydrocolloids* 15(4–6):383–400
64. Gil T, Sabra MC, Ipsen JH, Mouritsen OG. 1997. *Biophys. J.* 73(4):1728–41
65. Zhao X, Bartolucci G, Honigmann A, Jülicher F, Weber CA. 2021. *New J. Phys.* 23(12):123003
66. Rouches M, Veatch SL, Machta BB. 2021. *PNAS* 118(40):e2103401118
67. Beutel O, Maraspini R, Pombo-García K, Martin-Lemaitre C, Honigmann A. 2019. *Cell* 179(4):923–936.e11
68. Morin JA, Wittmann S, Choubey S, Klosin A, Golfier S, et al. 2022. *Nat. Phys.* 18(3):271–76
69. Renger R, Morin JA, Lemaitre R, Ruer-Gruss M, Jülicher F, et al. 2022. *PNAS* 119(10):e2107871119
70. Quail T, Golfier S, Elsner M, Ishihara K, Murugesan V, et al. 2021. *Nat. Phys.* 17(9):1007–12
71. Flory PJ. 1942. *J. Chem. Phys.* 10:51–61
72. Huggins ML. 1942. *J. Phys. Chem.* 46:151–58
73. Fritsch AW, Diaz-Delgadillo AF, Adame-Arana O, Hoege C, Mittasch M, et al. 2021. *PNAS* 118(37):e2102772118
74. Doi M, Edwards SF. 1988. *The Theory of Polymer Dynamics*. Oxford, UK: Clarendon
75. Rubinstein M, Colby RH. 2003. *Polymer Physics*. Vol. 23. New York: Oxford Univ. Press
76. Safran S. 2018. *Statistical Thermodynamics of Surfaces, Interfaces, and Membranes*. Boca Raton, FL: CRC
77. Lin YH, Forman-Kay JD, Chan HS. 2016. *Phys. Rev. Lett.* 117(17):178101
78. Lin YH, Song J, Forman-Kay JD, Chan HS. 2017. *J. Mol. Liquids* 228:176–93
79. McCall PM, Kim K, Fritsch AW, Iglesias-Artola J, Jawerth L, et al. 2020. bioRxiv:2020.10.25.352823
80. Saha S, Weber CA, Nousch M, Adame-Arana O, Hoege C, et al. 2016. *Cell* 166(6):1572–84
81. Pessina F, Giavazzi F, Yin Y, Gioia U, Vitelli V, et al. 2019. *Nat. Cell Biol.* 21(10):1286–99
82. Milo R, Phillips R. 2015. *Cell Biology by the Numbers*. New York: Garland Sci.
83. Mabillard J, Weber CA, Jülicher F. 2023. *Phys. Rev. E* 107:014118
84. Mittasch M, Gross P, Nestler M, Fritsch AW, Iserman C, et al. 2018. *Nat. Cell Biol.* 20(3):344–51
85. Jülicher F, Prost J. 2009. *Eur. Phys. J. E* 29:27–36
86. Wagner C. 1961. *Z. Elektrochem. Ber. Bunsenges. Phys. Chem.* 65(7–8):581–91
87. Lifschitz I, Slyozov V. 1961. *J. Phys. Chem. Solids* 19(1/2):35–50

88. Tjhung E, Nardini C, Cates ME. 2018. *Phys. Rev. X* 8(3):031080
89. Cates ME, Tjhung E. 2018. *J. Fluid Mech.* 836:P1
90. Grosberg AY, Joanny JF. 2015. *Phys. Rev. E* 92(3):032118
91. Ilker E, Joanny JF. 2020. *Phys. Rev. Res.* 2(2):023200
92. Landau LD, Lifshitz EM. 2013. *Fluid Mechanics: Landau and Lifshitz: Course of Theoretical Physics*, Vol. 6. New York: Elsevier
93. Arana OA. 2019. *Chemical control of liquid phase separation in the cell*. PhD Thesis, Tech. Univ. Dresden, Dresden, Germ.
94. Anderson JL. 1989. *Annu. Rev. Fluid Mech.* 21:61–99
95. Krüger S, Weber CA, Sommer JU, Jülicher F. 2018. *New J. Phys.* 20(7):075009
96. Weber C, Michaels T, Mahadevan L. 2019. *eLife* 8:e42315
97. Bo S, Hubatsch L, Bauermann J, Weber CA, Jülicher F. 2021. *Phys. Rev. Res.* 3(4):043150
98. Jawerth LM, Ijavi M, Ruer M, Saha S, Jahnel M, et al. 2018. *Phys. Rev. Lett.* 121(25):258101
99. Jawerth L, Fischer-Friedrich E, Saha S, Wang J, Franzmann T, et al. 2020. *Science* 370(6522):1317–23
100. Alberti S, Hyman AA. 2021. *Nat. Rev. Mol. Cell Biol.* 22(3):196–213
101. Boke E, Mitchison TJ. 2017. *Cell Cycle* 16(2):153–54
102. Woodruff JB, Hyman AA, Boke E. 2018. *Trends Biochem. Sci.* 43(2):81–94
103. Marrone L, Drexler HC, Wang J, Tripathi P, Distler T, et al. 2019. *Acta Neuropathol.* 138:67–84
104. Cahn JW. 1977. *J. Chem. Phys.* 66(8):3667–72
105. Gennes PG, Brochard-Wyart F, Quéré D, et al. 2004. *Capillarity and Wetting Phenomena: Drops, Bubbles, Pearls, Waves*. New York: Springer
106. De Gennes PG. 1985. *Rev. Mod. Phys.* 57(3):827–63
107. Nakanishi H, Fisher ME. 1982. *Phys. Rev. Lett.* 49(21):1565–68
108. Pandit R, Fisher ME. 1983. *Phys. Rev. Lett.* 51(19):1772–75
109. Schmidt JW, Moldover MR. 1983. *J. Chem. Phys.* 79:379–87
110. Kellay H, Bonn D, Meunier J. 1993. *Phys. Rev. Lett.* 71:2607–10
111. Kusumaatmaja H, May AI, Knorr RL. 2021. *J. Cell Biol.* 220(10):e202103175
112. Aumeier C. 2022. *Biophys. J.* 121(3):3a
113. Rao M, Mayor S. 2014. *Curr. Opin. Cell Biol.* 29:126–32
114. Cebecauer M, Amaro M, Jurkiewicz P, Sarmento MJ, Sachl R, et al. 2018. *Chem. Rev.* 118(23):11259–97
115. Lipowsky R. 2023. *Membranes* 13(2):223
116. Lu T, Liese S, Schoenmakers L, Weber CA, Suzuki H, et al. 2022. *J. Am. Chem. Soc.* 144(30):13451–55
117. Agudo-Canalejo J, Schultz SW, Chino H, Migliano SM, Saito C, et al. 2021. *Nature* 591(7848):142–46
118. Hernández-Vega A, Braun M, Scharrel L, Jahnel M, Wegmann S, et al. 2017. *Cell Rep.* 20(10):2304–12
119. Setru SU, Gouveia B, Alfaro-Aco R, Shaevitz JW, Stone HA, Petry S. 2021. *Nat. Phys.* 17(4):493–98
120. Quéré D, Di Meglio JM, Brochard-Wyart F. 1990. *Science* 249(4974):1256–60
121. Wegmann S, Eftekharzadeh B, Tepper K, Zoltowska KM, Bennett RE, et al. 2018. *EMBO J.* 37(7):e98049
122. Ukmar-Godec T, Wegmann S, Zweckstetter M. 2020. *Semin. Cell Dev. Biol.* 99:202–14
123. Kim Y, Shi Z, Zhang H, Finkelstein IJ, Yu H. 2019. *Science* 366(6471):1345–49
124. Golfier S, Quail T, Kimura H, Brugués J. 2020. *eLife* 9:e53885
125. Deleted in proof
126. Sear RP, Cuesta JA. 2003. *Phys. Rev. Lett.* 91(24):245701
127. Jacobs WM, Frenkel D. 2017. *Biophys. J.* 112(4):683–91
128. Shrinivas K, Brenner MP. 2021. *PNAS* 118(45):e2108551118
129. Jacobs WM, Frenkel D. 2013. *J. Chem. Phys.* 139(2):024108
130. Zwicker D, Laan L. 2022. *PNAS* 119(28):e2201250119
131. Ong SE, Mann M. 2005. *Nat. Chem. Biol.* 1(5):252–62
132. Semenov AN, Rubinstein M. 1998. *Macromolecules* 31(4):1373–85
133. Choi JM, Dar F, Pappu RV. 2019. *PLOS Comput. Biol.* 15(10):e1007028
134. Choi JM, Holehouse AS, Pappu RV. 2020. *Annu. Rev. Biophys.* 49:107–33
135. Bremer A, Farag M, Borcherds WM, Peran I, Martin EW, et al. 2022. *Nat. Chem.* 14(2):196–207
136. Guillén-Boixet J, Kopach A, Holehouse AS, Wittmann S, Jahnel M, et al. 2020. *Cell* 181(2):346–61

137. Kar M, Dar F, Welsh TJ, Vogel LT, Kühnemuth R, et al. 2022. *PNAS* 119(28):e2202222119
138. Patel A, Malinovska L, Saha S, Wang J, Alberti S, et al. 2017. *Science* 356(6339):753–56
139. Blankschtein D, Thurston GM, Benedek GB. 1985. *Phys. Rev. Lett.* 54(9):955
140. Tanaka F. 2011. *Polymer Physics: Applications to Molecular Association and Thermoreversible Gelation*. Cambridge, UK: Cambridge Univ. Press. 1st ed.
141. Deviri D, Safran SA. 2020. *Soft Matter* 16(23):5458–69
142. Bartolucci G, Haugerud IS, Michaels TCT, Weber CA. 2023. bioRxiv:2023.04.18.537072. **https://www.biorxiv.org/content/10.1101/2023.04.18.537072v3**
143. Dimura M, Peulen TO, Hanke CA, Prakash A, Gohlke H, Seidel CA. 2016. *Curr. Opin. Struct. Biol.* 40:163–85
144. Michaels TC, Mahadevan L, Weber CA. 2022. *Phys. Rev. Res.* 4(4):043173
145. Pönisch W, Michaels TC, Weber CA. 2023. *Biophys. J.* 122:197–214
146. Welsh TJ, Krainer G, Espinosa JR, Joseph JA, Sridhar A, et al. 2022. *Nano Lett.* 22(2):612–21
147. Scott E, Tung L, Drickamer H. 1951. *J. Chem. Phys.* 19(9):1075–78
148. Auer P, Murbach E. 1954. *J. Chem. Phys.* 22(6):1054–59
149. Zhang Y, Pyo AGT, Jiang Y, Brangwynne CP, Stone HA, Wingreen NS. 2022. bioRxiv:2022.03.16.484641
150. Wanger C. 1961. *Z. Elektrochem.* 65:581–91
151. Folkmann AW, Putnam A, Lee CF, Seydoux G. 2021. *Science* 373(6560):1218–24
152. Cochard A, Navarro MGJ, Piroska L, Kashida S, Kress M, et al. 2022. *Biophys. J.* 121(9):1675–90
153. Goldberg GS, Valiunas V, Brink PR. 2004. *Biochim. Biophys. Acta (BBA)-Biomembranes* 1662(1–2):96–101
154. Krug SM, Schulzke JD, Fromm M. 2014. *Semin. Cell Dev. Biol.* 36:166–76